Appendix B: Indentation Contact Hardness

This appendix will address the second parameter (*e.g.* in addition to elastic modulus) that is frequently reported following an indentation test, the contact hardness. The historical linkage between Vickers indentation tests—used to assess plastic deformation in metals—and nanoindentation is reviewed. The contact hardness is considered analytically using series deformation models for both elastic-plastic and viscous-elastic-plastic indentation. Relationships between contact hardness and elastic modulus are considered. A new technique is developed to use contact hardness measurements to explicitly evaluate time-dependence in a material.

B.1 Contact Hardness Background

B.1.1 Vickers Indentation

In nanoindentation studies on engineering materials, particularly with metallic samples but also with glass or ceramic materials, the contact hardness is a frequently reported parameter. This is, at least in part, historical—the contact hardness is a well-understood quantity for metals, as measured using the Vickers hardness test and related to the metal's yield stress [Tabor, 1951]. For biological materials, although there have been studies published investigating the Vickers hardness, in the nanoindentation literature the contact hardness has tended to be dismissed as being a linear function of the elastic modulus and thus not an independent property [Zysset et al, 1999; Cheng et al, 2003b]. For metals, since the contact hardness (including the Vickers hardness or nanoindentation hardness) is associated with the yield strength of metals, people associate hardness measurements with a resistance to plastic deformation. This is confirmed with the difference between contact hardness values for very different materials with similar modulus values but different plastic deformation responses, such as fused silica (H_c ~ 9-10 GPa) with essentially no plastic deformation and aluminum (H_c ~ 0.25 GPa) with dominant plastic deformation. In this section a framework is developed for examination of the meaning of contact hardness, its association with plastic deformation resistance, laying the groundwork for examination of mineralized tissues' mechanical behavior later in this chapter.

Contact hardness, H_c, is defined as

$$H_C = \frac{P_{MAX}}{A_R} \qquad \text{[B-1]}$$

where P_{MAX} is the indentation peak load and A_R is the residual contact impression area. In a traditional hardness test, the residual impression is measured by optical microscopy following the loading (Figure B-1).
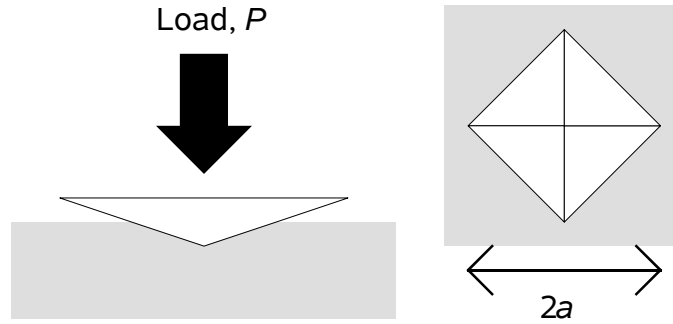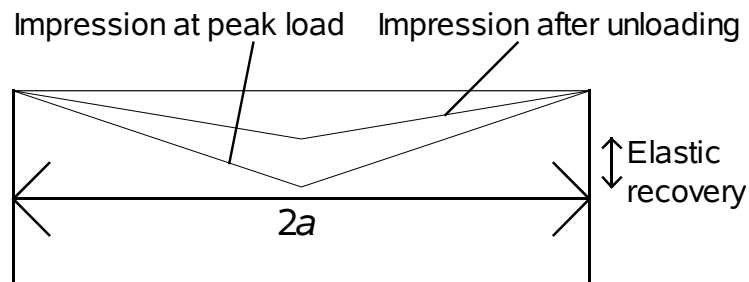
Figure B-1: Vickers Indentation schematic illustration. (Left) transverse section of the loading event; (right) top-down examination of the residual impression. The diagonal length is measured as 2*a*.

The hardness is then calculated as

$$H_C = \frac{P_{\text{MAX}}}{2a^2}$$ [B-2]

where 2*a* is the diagonal length of the impression. Although usually associated with plastic deformation, since it was commonly used for metals where the plastic deformation was substantial, the residual impression does in fact result from both elastic and plastic deformation during the contact. It is assumed that the residual impression is fixed and does not change on unloading, and that the elastic recovery occurs in the depth direction only (Figure B-2):


Figure B-2: Schematic illustration of elastic recovery in a transverse section of an indentation impression.

B.1.1 Contact Hardness in Nanoindentation

In depth-sensing indentation testing, the indent impression is frequently too small to be measured optically, and the residual impression is thus not measured but the area is inferred from the assumption that the residual area is the same as the contacted area at maximum load, A_c which is in turn calculated from the contact depth h_c.

$$H_C = \frac{P_{MAX}}{A_C} = \frac{P_{MAX}}{\alpha_1 (h_C)^2}$$ [B-3]

where α_1 is 24.5 for an ideal Vickers or Berkovich indenter. This assumption, that the inferred contact area approximates the residual area, can be verified by comparing nanoindentation measurements of the contact hardness with Vickers indentation measurements. In this work, comparisons were made for hydroxyapatite and for a gelatin-apatite composite, both indented with a nanoindenter and with a Vickers microindenter. The residual Vickers impressions for both materials are shown in Figure B-3. There was substantial shear faulting but no cracking in the composite material and there was significant cracking in the apatite.
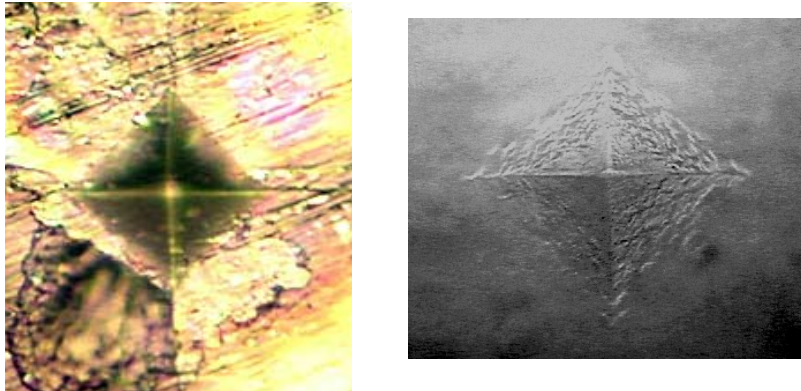
Figure B-3: (left) Vickers indentation residual impression in hydroxyapatite. Indentation force was 4.9 N. Image has been contrast enhanced. Cracking is also visible. (right)Vickers indentation residual impression in composite C. Indentation force was 9.8 N. Image has been contrast enhanced.

The contact hardness values for nanoindentation testing at mN-level peak loads are presented along with the microindentation Vickers hardness numbers (obtained at N-level loads) for both materials in Figure B-4. Clearly the large load limits of the nanoindentation data, with areas inferred from the calibration, are in good agreement with the small load limit of the Vickers indentation data, from optical area measurements. At small loads, the nanoindentation contact hardness values increase with decreased peak load level, an effect that has been frequently observed in metals and polymers (although poorly understood) and is known as the indentation size effect [Nix and Gao, 1998].
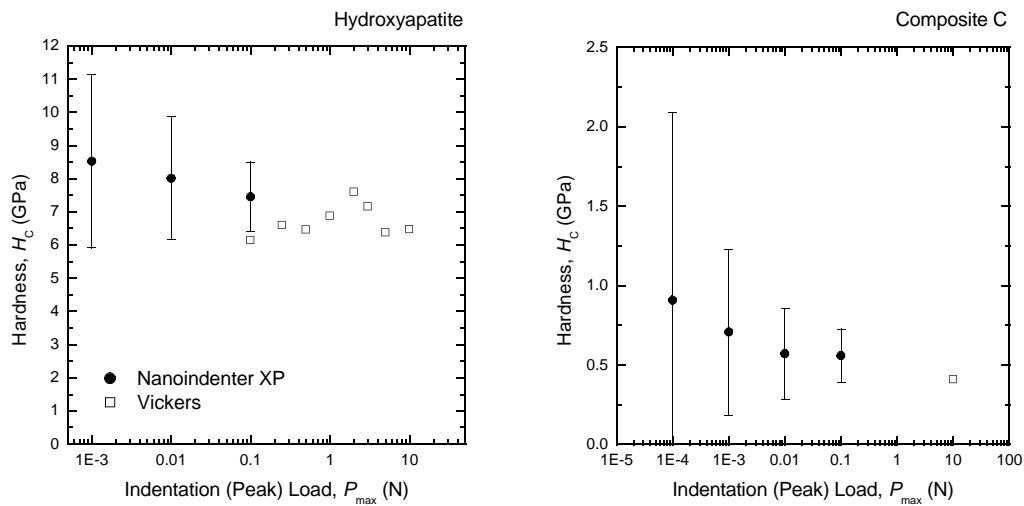
Figure B-4: Contact hardness (H_c) for (left) hydroxyapatite and (right) gelatin-apatite composite "C" as a function of indentation peak load for both nanoindentation and Vickers indentation. The solid symbols are for nanoindentation and the open symbols are for Vickers indentation.

B.2 Elastic-Plastic Contact Hardness

B.2.1 Series Model

As stated above, both elastic and plastic deformations contribute to both the formation of a residual indentation impression or to the total contact area at peak load [Sakai, 1999]. If the elastic (h_E) and plastic (h_P) deformations are assumed to contribute to the total contact displacement (h_c) as mechanical elements in series such that the displacements sum:

$$h_c = h_E + h_P \qquad \text{[B-4]}$$

where the known form of the elastic load-displacement relation is

$$P_E = \alpha_2 E' h_E^2 \qquad \text{[B-5]}$$

where $\alpha_2 = 4.4$ for a Berkovich indenter (from Eqn 3-10) and P_E is the load in the elastic element. The form of the plastic deformation element is

$$P_P = \alpha_1 H h_P^2 \qquad \text{[B-6]}$$

where $\alpha_1 = 24.5$ for a Berkovich indenter and P_P is the load in the elastic element. Knowing that for elements in series the loads are equal $(P_E = P_P)$ then the contact hardness can be written by combining equations B-3 to B-6:

$$H_c = \frac{1}{\alpha_1 \left((\alpha_2 E')^{-1/2} + (\alpha_1 H)^{-1/2} \right)^2} \qquad \text{[B-7]}$$

B.2.2 Elastic-Plastic Materials Analysis

B.2.2.1 Engineering Materials

The resistance to plastic deformation, H, was calculated numerically for a variety of materials from E' and H_c values obtained in an indentation test (Table B-1; numerical values from [Oliver and Pharr, 1992] and experiments performed by myself). The relative contributions of elastic and plastic deformation to the overall indentation response can then be calculated for the elastic-plastic materials by calculating the elastic and plastic deformation components using Eqns. B-5 and B-6 from the properties E' and H (Table B-2). As would be expected, fused silica glass and sapphire ceramic are dominated by elastic deformation, metals by plastic deformation, and interestingly apatite and enamel (which is mostly apatite) are near 50-50 in the balance of elastic and plastic deformation.

Table B-1: Plastic deformation resistance H calculated from modulus E' and contact hardness H_c from Eqn. B-7.

material	Plane strain modulus, E' (GPa)	Contact Hardness, H_c (GPa)	Plastic Deformation Resistance, H*
fused silica	70	9.2	450
sapphire	400	30	240
tungsten	410	4	7
aluminum	70	0.25	0.34
enamel	100	4	15
apatite	155	7.2	30

*a value of γ = 1 (see section 3.1.2.2) was assumed in calculating H

Table B-2: Relative proportions of elastic and plastic deformation (h_E, h_P) calculated from the values in Table B-1 for P_{max} 10 mN.

| material	Elastic deformation, h_E nm, (%)	Plastic deformation, h_P nm, (%)
fused silica	180 (86%)	30 (14%)
sapphire	75 (65%)	41 (35%)
Tungsten	74 (23%)	241 (77%)
aluminum	180 (14%)	1096 (86%)
enamel	151 (48%)	165 (52%)
apatite	121 (51%)	117 (49%)

B.2.2.2 Dentin

This hardness analysis was next considered for mineralized tissues. The dentin-enamel junction data from section 3.4.1 was further explored via quantitative analysis of the rows of indentation results.

Based on the optical images and indent locations (Figure 3-22), each indentation was assigned to being solely on dentin, solely on enamel, and on the junction region. The indents (1 or 2 per line) on the junction region for each line were assigned a zero value for approximate distance from the DEJ. Indents at other locations in each row (*e.g.* not lying directly on the DEJ) were assigned coordinate values in multiples of 100 μm (the inter-indent spacing in the x-direction) to represent their approximate distance from the DEJ. Averages and standard deviations for modulus and contact hardness at each distance interval were calculated, and are presented in Figure B-5 for both dentin and enamel.

Different trends in modulus and contact hardness for the dentin and enamel were evident. Dentin contact hardness and enamel modulus showed a clear and steady trend with increasing property values with distance from the DEJ. Dentin modulus showed a slight increase (8.5% difference between 100 and 1200 μm), a factor of two less steep than that for the contact hardness (16.2% difference in the same range). Enamel

demonstrated approximately the same total increase in E' and H_c with distances from 100 to 900 mm from the DEJ (~ 15% in both cases) but the pattern of change with distance in contact hardness was not smoothly increasing with distance as it was for modulus.
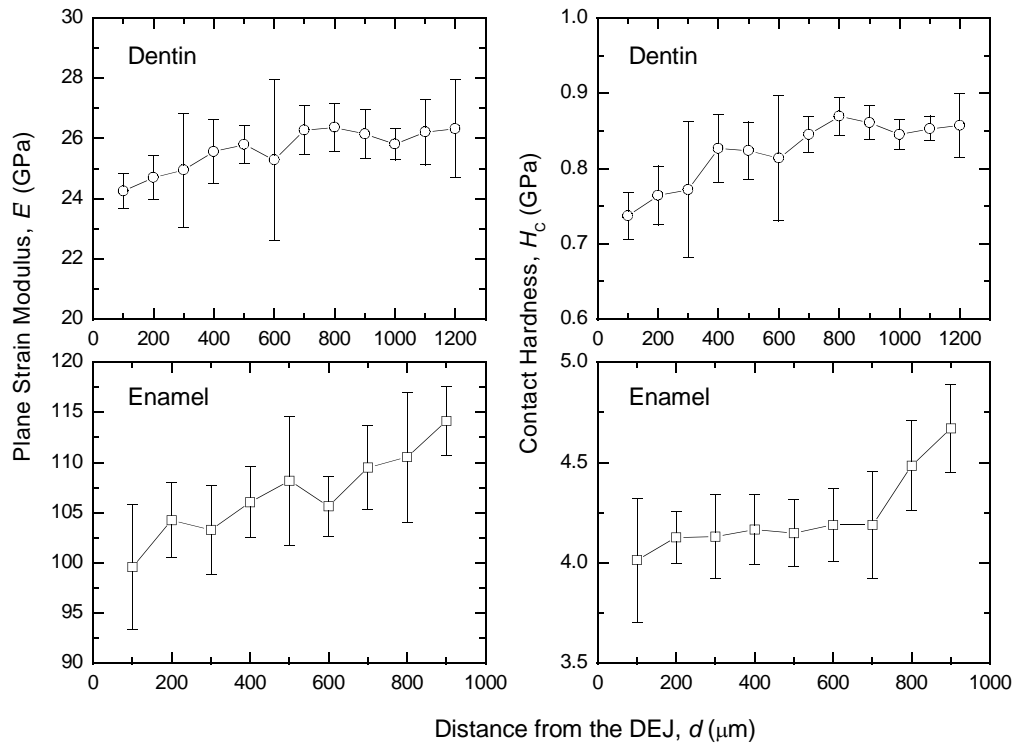
Figure B-5: Property gradients with distance from the dentin enamel junction for dentin and enamel.

The modulus map (Figure 3-22), and the quantitative evaluation of the modulus data (Figure B-5) also demonstrate an intriguing gradient in dentin modulus near the DEJ. To examine the transition region nearest the DEJ, the data were grouped and averages computed for indents in the very-near region (100 or 200 μm from the DEJ) compared to those in the far region (300 or more μm from the DEJ) These means and standard deviations are presented in Table B-3.

Table B-3: Property averages for indentation tests performed near to and far from the DEJ region for dentin and enamel indentation testing.

	Modulus, E' (GPa)	Hardness, Hc (GPa)
Enamel, near $(d \le 200\,\mu m)$	101.9 ± 5.6	4.07 ± 0.24
Enamel, far $(d \ge 300\,\mu m)$	107.0 ± 5.2	4.21 ± 0.24
Enamel ratio, near region/far region	0.95	0.97
Dentin, near $(d \le 200\,\mu m)$	24.5 ± 0.7	0.75 ± 0.04
Dentin, far $(d \ge 300\,\mu m)$	25.9 ± 1.4	0.84 ± 0.05
Dentin ratio, near region/far region	0.95	0.89

The greatest change was in the contact hardness of dentin, which dropped by more than 10% in the region nearest the DEJ. Since the modulus also changed slightly in the same region, it was desired that the effect of modulus and plastic deformation resistance be considered independently. Average plastic deformation resistance (H) was calculated from average E' and H_c using equation B-7, and presented in Table B-4. The plastic deformation resistance (H) for dentin in the near-DEJ region is depressed 15% compared to the distant dentin values. It is this large change, combined with a small (5%) change in the elastic modulus, that contribute to the 11% decrease in contact hardness data for the same comparison.

Table B-4: Plastic deformation resistance (H) calculated from the plane strain modulus (E') and contact hardness (H_c) data presented in Table B-3.

Plastic deformation resistance, H (GPa)	Dentin	Enamel
near region $(d \le 200\,\mu m)$	2.18	14.6
far region $(d \ge 300\,\mu m)$	2.55	14.9
ratio, near region/far region	0.85	0.98

The results of the current investigation are consistent with those seen previously, in a contact hardness study of the DEJ [White et al, 2000] indicating a broad transition region ~ 100 microns wide across the DEJ (large relative to the optically visible junction

region of about 2 microns); and differences in the enamel and dentin near the junction when compared to the bulk.

The elastic modulus and plastic deformation resistance are showing different patterns in this study, indicating substantial differences between the modes of elastic and plastic deformation in the mineralized tissue dentin. Further study of these results may prove extremely useful in gaining understanding of the structure and function of the dentin-enamel junction.

B.2.2.3 Considerations for Bone

It has been reported experimentally [Zysset et al, 1999; Chang et al, 2003b] for bone samples that the contact hardness is an approximately linear function of the elastic modulus. A plot can be generated to examine this analytically for constant values of the plastic deformation resistance H, to demonstrate the effect of changes in the elastic modulus E' on the perceived contact hardness, H_c (Figure B-6, left). If the value of plastic deformation resistance H is held fixed at 1 GPa (a good approximation for bone; section 4.4.2) and modulus is varied over a bone-like range, from 10-30 GPa, then a linear approximation is a reasonably good approximation of the full E'-H_c behavior in this limited modulus range (Figure B-6, right).

If, in fact, the plastic deformation resistance is found to increase with plane strain modulus, instead of being constant, then the contact hardness would be an explicit linear function of the modulus (as opposed to a linear approximation in a limited range, as in Figure B-6). However, given the limited range of modulus values observed (say from 10-30 GPa for bone) it would be difficult to make this distinction in experimental data.
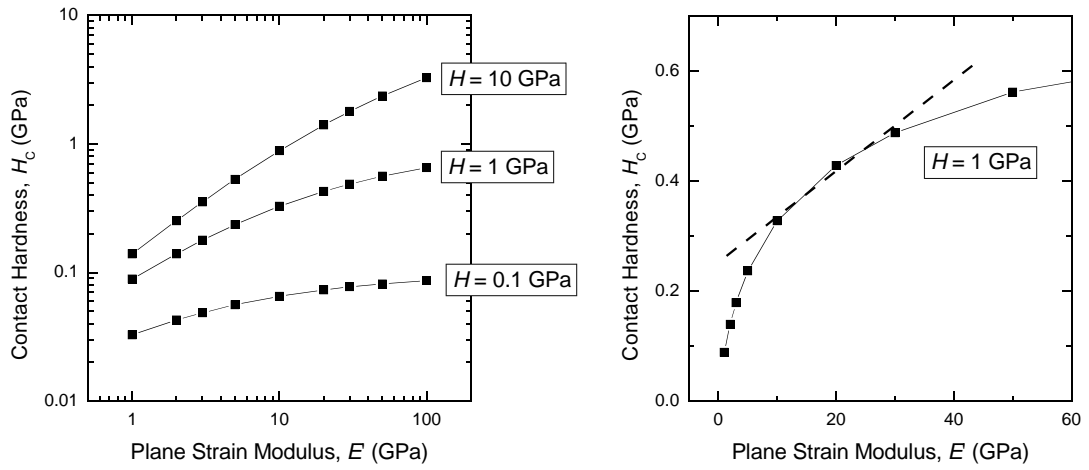
Figure B-6: (left) Calculated contact hardness (H_c, Eqn. B-7) versus plane strain modulus (E') for three different values of the plastic deformation resistance, H. (right) Over an experimentally-observed range of bone modulus values (10-30 GPa) and a bone-like H (1 GPa) the contact hardness (H_c) appears to increase approximately linearly with modulus (dashed line).

B.3 Viscous-Elastic-Plastic Contact Hardness

B.3.1 Series Model

We return to the discussion of the meaning of the contact hardness parameter H_c in indentation testing, particularly within the context of materials exhibiting time-dependent deformation. In agreement with the formulation of the VEP model (section 4.3), we can rewrite the total displacement with the addition of a time-dependent series contribution from viscous deformation (h_V):

$$h_c = h_V + h_E + h_P \qquad\qquad \text{[B-8]}$$

where

$$h_V = h_V(t) \qquad\qquad \text{[B-9]}$$

The addition of this viscous deformation component causes the contact hardness to be an explicit function of time $\quad H_c = H_c(t) \quad$ and can be written

$$H_c(t) = \frac{1}{\alpha_1\left((\alpha_2 E')^{-1/2} + (\alpha_1 H)^{-1/2} + f(t)\right)^2} \qquad\qquad \text{[B-10]}$$

where $f(t)$ depends on the model chosen for the material viscoelasticity. For the VEP model (section 4.3) this can be written in terms of the experimental rise time t_R:

$$H_c(t_R) = \frac{1}{\alpha_1\left((\alpha_2 E')^{-1/2} + (\alpha_1 H)^{-1/2} + (2 t_R/3)(\alpha_3 \eta_Q)^{-1/2}\right)^2} \qquad\qquad \text{[B-11]}$$

or, restated as an explicit function of the ratio of rise time (t_R) and material time constant τ_Q :

$$H_c(t_R) = \frac{1}{\alpha_1\left(\left(\alpha_2 E'\right)^{-1/2} + \left(\alpha_1 H\right)^{-1/2} + \left(2 t_R / 3 \tau_Q\right)\left(\alpha_2 E'\right)^{-1/2}\right)^2}$$

$$= \frac{1}{\alpha_1\left(\left(\alpha_2 E'\right)^{-1/2}\left[1 + 2 t_R / 3 \tau_Q\right] + \left(\alpha_1 H\right)^{-1/2}\right)^2} \qquad \text{[B-12]}$$

B.3.2 Estimation of Material Time-Constant from Contact Hardness

For fixed plane strain elastic modulus (E') and plastic deformation resistance (H), the contact hardness H_c is plotted in Figure B-7 as a function of experimental rise time t_R for materials with four different values of the VEP time constant τ_Q (24, 75, 238, 754 s).
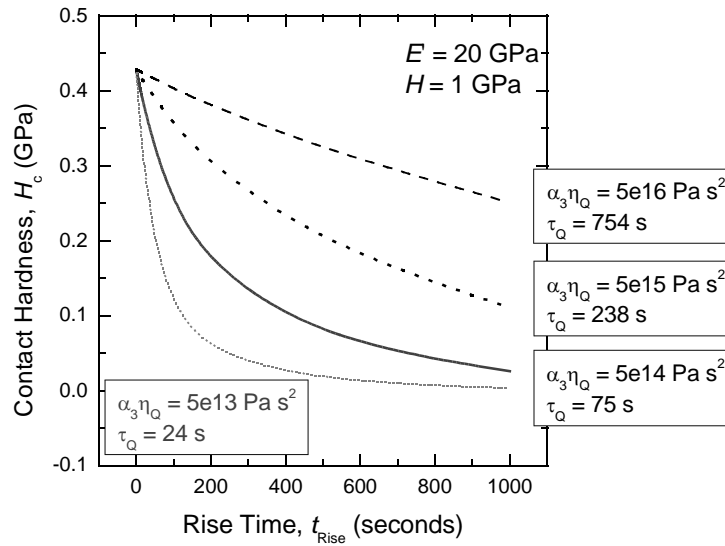
Figure B-7: Plot of calculated contact hardness versus experimental rise time (H_c-t_R) for four different values of the viscosity (or time constant) at fixed modulus (E') and plastic deformation resistance (H).

281

Interestingly, a reasonably (better than order-of-magnitude) estimate for the material time constant can be obtained by fitting the contact hardness-rise time (H_c-t_R) data (Figure B-7) to an exponential decay function of the form $y = A \exp(-t/\tau)$. The time-constant (τ) values obtained from the exponential fit to data in Figure B-7 are shown in Table B-5. The exponential fit coefficient τ was on the order of, but consistently higher than, the known (input) VEP time constant τ_Q, by approximately a factor of two.

Table B-5: Time constants (known) and exponential decay constant fits for the H_c-t_R data shown in Figure B-7.

Time constant, τ_Q (s)	Exponential decay constant from fitting H_c-t_R data, τ (s)	Ratio, decay constant to VEP time constant τ/τ_Q
24	63	2.63
75	176	2.35
238	460	1.93
754	1235	1.64

Experimental contact hardness values for two polymeric materials (polycarbonate, PC, and high-density polyethylene, HDPE) are shown in Figure B-8 for rise times (t_R) from 10 to more than 3000 seconds. The data were fit to an exponential as above, and the time constants were found to be $\tau = 118$ and $\tau = 285$ seconds for HDPE and PC, respectively. These values compare well to the VEP time constant values reported for these materials ($\tau_Q = 685$ s for PC and $\tau_Q = 143$ s for HDPE) based on direct fits of the indentation load-displacement (P-h) responses to the VEP model [Oyen and Cook, 2003].

Therefore, an interesting mechanism is here proposed and demonstrated for the nonspecialist to estimate a viscoelastic time constant. An extremely simple experiment can be performed, a series of indentation tests utilizing loading and unloading at constant rate, varying the rise time over a considerable range. A single fit can then be made to the plot of contact hardness versus rise time (H_c-t_R) as shown in Figure B-8. The obtained time constant (τ) values are sufficient for simple material- or treatment-based

comparisons, but not meant to be confused with a rigorous method for viscoelastic analysis.
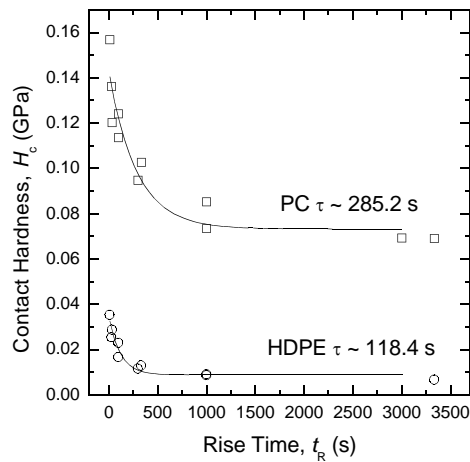
Figure B-8: Oliver-Pharr contact hardness (H_c) as a function of rise time (t_R) for polycarbonate (PC) and high-density polyethylene (HDPE) plastics. The lines are an exponential decay fit, giving estimated material time constants that compare favorably with those measured by VEP curve fits (685 for PC and 143 for HDPE).

B.3.3 Contact Hardness Calculations for Time-Dependent Materials

B.3.3.1 PL-1 Polymer

The contact hardness is calculated using Eqn. B-12 for PL-1 polymer at different load levels, based on the parameters obtained in VEP fits (Table 4-1). Results are shown in Table B-6; the contact hardness shows the same gradual decrease with indentation load as was seen previously for the elastic modulus (Figure 3-9).

Table B-6: H_c calculated for PL-1 using VEP model and Eqn. B-12 using data in Table 4-1 for results at different load levels.

P_{max} (mN)	E (GPa)	H (GPa)	H_c (GPa)
0.3	3.63 ± 0.34	4.86 ± 2.17	0.32
1	3.40 ± 0.34	4.57 ± 3.95	0.30
3	3.69 ± 0.20	1.97 ± 0.37	0.25
10	3.43 ± 0.17	1.71 ± 0.25	0.23
30	3.05 ± 0.02	1.42 ± 0.07	0.20
100	2.72 ± 0.10	1.35 ± 0.04	0.19
300	2.50 ± 0.11	1.48 ± 0.10	0.18

B.3.3.2 Bone

For bone experiments performed in the current study (section 4.4.2), the VEP parameter describing resistance to plastic deformation (H) is not a direct function of the elastic modulus (Figure B-9, left). For these same bone indentation tests, the contact hardness can be calculated by Eqn. B-12 for each test. Consistent with previously-reported observations [Chang et al, 2003; Zysset et al, 1999] , the calculated contact hardness (H_c) increases with elastic modulus (Figure B-9, right; $p < 0.01$ from linear regression). The average calculated contact hardness value was found to be 0.43 GPa. This value is quantitatively in good agreement with results previously reported for dry bone [Rho et al, 1997].

One advantage to calculating the contact hardness from the E, H, t_R and η_Q values instead of inferring it from load-displacement directly is that the infinitely fast (zero t_R) elastic-plastic contact hardness can also be calculated and used to assess the influence of time-dependent deformation in the indentation time frame. For the healing bone study (section 4.4.2) study the zero t_R contact hardness averaged 0.48 GPa. Thus, although the time-dependent deformation appeared to make a relatively small contribution to the indentation response, this mode of deformation did substantially affect the perceived contact hardness, by more than 10% in the current study.
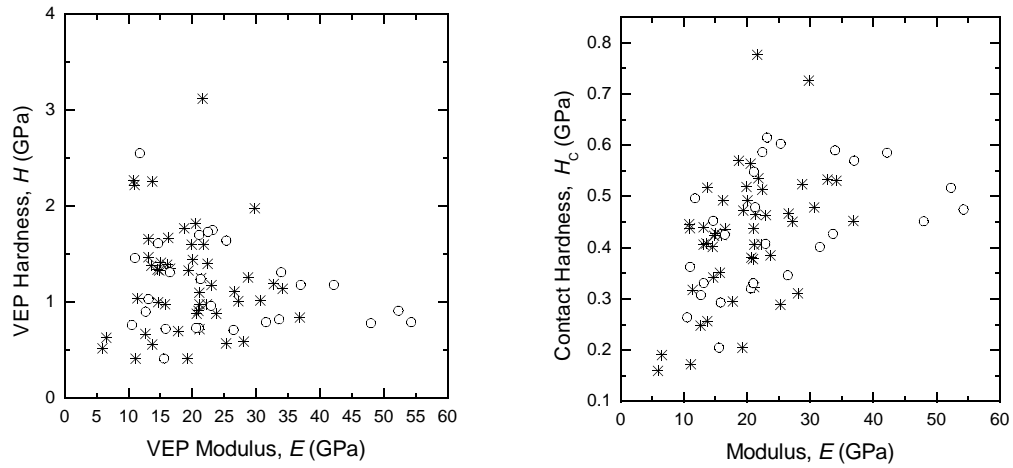
Figure B-9 (left) There is no direct relationship between the modulus (E) and plastic deformation resistance (H) terms obtained by VEP deconvolution of indentation load-displacement traces. (right) The calculated contact hardness (H_c, from Eqn. B-12) increases significantly with elastic modulus.